PHYSICAL REVIEW B **84**, 064433 (2011)

# $\mu$SR investigation of magnetism and magnetoelectric coupling in $Cu_2OSeO_3$

A. Maisuradze,[1,2,*] Z. Guguchia,[1] B. Graneli,[1,3] H. M. Rønnow,[4] H. Berger,[4] and H. Keller[1]
[1]*Physik-Institut der Universität Zürich, Winterthurerstrasse 190, CH-8057 Zürich, Switzerland*
[2]*Laboratory for Muon Spin Spectroscopy, Paul Scherrer Institut, CH-5232 Villigen PSI, Switzerland*
[3]*Institute of Theoretical Physics, ETH Hönggerberg, CH-8093 Zürich, Switzerland*
[4]*Institute of Condensed Matter Physics, École Polytechnique Fédérale de Lausanne (EPFL), CH-1015 Lausanne, Switzerland*
(Received 30 April 2011; revised manuscript received 8 July 2011; published 26 August 2011)

A detailed zero- and transverse-field muon spin rotation investigation of magnetism and the magnetoelectric coupling in $Cu_2OSeO_3$ is reported. An internal magnetic field $B_{int}(T = 0) = 85.37(25)$ mT was found, in agreement with a ferrimagnetic state below $T_c = 57.0(1)$ K. The temperature dependence of the magnetic order parameter is well described by the relation $B_{int} = B(0)(1 - (T/T_c)^2)^{\tilde{\beta}}$ with an effective exponent $\tilde{\beta} \simeq 0.39(1)$, which is close to the critical exponent $\beta \simeq 1/3$ for a three-dimensional (3D) magnetic system. Just above $T_c$ the muon relaxation rate follows the power law $\lambda(T) \propto (T/T_c - 1)^{-\tilde{\omega}}$ with $\tilde{\omega} = 1.06(9)$, which is characteristic for 3D ferromagnets. Measurements of $B_{int}(T)$ with and without an applied electrostatic field $E = 1.66 \times 10^5$ V/m suggest a possible electric-field effect of magnitude $\Delta B_V = B_V(0\ \text{V}) - B_V(500\ \text{V}) = -0.4(4)$ mT.

DOI: 10.1103/PhysRevB.84.064433 PACS number(s): 75.85.+t, 75.50.Gg, 76.75.+i

## I. INTRODUCTION

Much attention has been directed toward multiferroic and magnetoelectric materials in recent years.[1–4] The coupling between magnetic and electric parameters increases the degrees of freedom of the ordered ground state, making these materials good candidates for the study of new phenomena in highly correlated electronic systems. Strong magnetoelectric coupling is rather rare in the solid state, since the usual microscopic mechanisms for magnetic and electric polarization are mutually exclusive. Magnetism requires strong exchange interactions related to a strong hybridization of the transition ion electrons leading to conductivity. Conductivity, on the other hand, is inconsistent with the presence of an electric polarization in a sample.[5] It is therefore of particular importance to unravel the mechanisms behind magnetoelectric coupling. A number of atomic mechanisms have been proposed in order to explain the magnetoelectric coupling.[1,6–8] Considering spatial and time inversion symmetry for magnetic (**M**) and electric (**P**) polarization, it was concluded that linear magnetoelectric coupling is only possible when both vectors vary in space and time.[4] On the other hand, the importance of frustration effects in magnetoelectrics for the static polarizations of **P** and **M** was stressed for nonlinear coupling mechanisms.[4] The presence of large magnetic and electric polarizations is an important condition for strong magnetoelectric coupling, making ferro- or ferrimagnetic materials favorable candidates.[1]

The ferrimagnetic magnetoelectric compound $Cu_2OSeO_3$ was recently discovered,[9,10] and single crystals were successfully grown soon afterward.[11] The compound is piezoelectric and undergoes a ferrimagnetic transition below 60 K, exhibiting magnetoelectric coupling as revealed by magnetocapacitance studies on a polycrystalline sample.[9] An abrupt change of the dielectric constant below the ferrimagnetic transition was later confirmed by infrared studies.[12,13] At present the nature of the magnetoelectric coupling is unknown, since the most common mechanisms, involving magnetostriction and piezoelectric effects via lattice distortions, are excluded. Neither x-ray diffraction[9] nor nuclear magnetic resonance[11] studies revealed any lattice anomaly below the Néel temperature.

The positive muon is a very sensitive microscopic probe for studying magnetic properties in a zero as well as in an applied electric field.[14] Following the pioneering works of Eschchenko *et al.*[15] and Lewtas *et al.*,[16] we implemented a setup with alternating electric fields and performed a muon spin rotation/relaxation ($\mu$SR) investigation of magnetism and magnetoelectric coupling in $Cu_2OSeO_3$. The temperature dependence of the internal magnetic field $B_{int}$ was investigated below $T_c = 57.0(1)$ K, and the relaxation rate was studied above $T_c$. Zero-field (ZF) $\mu$SR measurements of the internal-field distribution with and without an applied electric field $E = 1.66 \times 10^5$ V/m indicate a small electric-field effect on the internal magnetic field: $\Delta B_V = B_V(0\ \text{V}) - B_V(500\ \text{V}) = -0.4(4)$ mT.

The paper is organized as follows: The sample preparation and the details of experimental setup are described in Sec. II. In Sec. III we describe the model used for analysis of the $\mu$SR data and the relation of the measured $\mu$SR spectrum to the lattice and magnetic structure of the sample. In Sec. IV we present and discuss the obtained results. Conclusions are given in Sec. V.

## II. EXPERIMENTAL DETAILS

A high-quality single crystal of $Cu_2OSeO_3$ of approximate size $7 \times 8 \times 3$ mm$^3$ was prepared in a manner described elsewhere.[11] ZF and transverse-field (TF) $\mu$SR experiments were performed at the $\pi$E3 beam line at the Paul Scherrer Institute (Villigen, Switzerland). The crystal structure is cubic with symmetry ($P2_13$).[9,10] The sample was aligned with its (100) direction parallel to the incident muon beam. The top side of the crystal pointing toward the incident beam (see Fig. 1) has two faces, which are canted at approximately $+30°$ and $-30°$ with respect to the (100) direction. The spin vector of the muon was oriented approximately at an angle of 60° with respect to the momentum vector. The asymmetry time spectra were monitored in the "Forward," "Backward," "Up," and "Down" (FBUD) positron detectors.[14] Typical statistics was 40–50 $\times 10^6$ positron events in the FBUD detectors for a

 

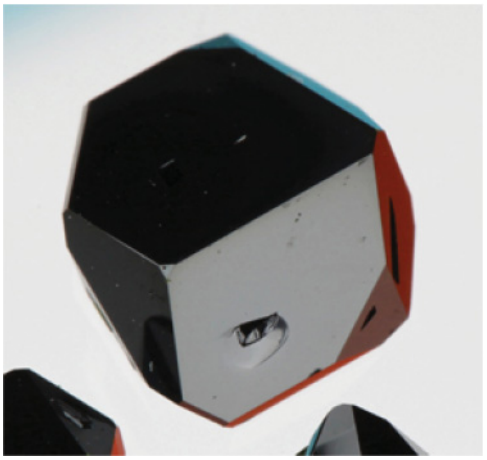

FIG. 1. (Color online) View of the measured $Cu_2OSeO_3$ crystal from the direction of the incident muon beam [the (100) direction]. Two faces, at angles of approximately $+30^\circ$ and $-30^\circ$ from the (100) direction, are visible.

spectrum with a 5-$\mu$s time window. The switched electric field $E$ was applied along the (100) direction of the 3-mm-thick crystal. The crystal was mounted between two parallel Cu electrodes: A thin (50-$\mu$m) Cu metal foil was used as the positive electrode, and the negative electrode was soldered to the sample holder and electrically connected to ground. The dielectric constant $\epsilon = 14.3$ has been reported for $Cu_2OSeO_3$.[9] Therefore, the electric-field polarization (**P**) has a distribution around the (100) direction due to canted faces of the crystal (see Fig. 1), since **P** tends to be normal to the faces. The applied voltage was switched at a rate of 100 Hz for two reasons: (i) to avoid accumulation of muon-created charge in the vicinity of the sample-to-electrode contact surface, which might offset and even cancel the applied field $E$; and (ii) to provide a well-defined consecutive reference in order to reduce artifacts related to any slight variation in temperature or applied magnetic field with time. All positron events registered by the FBUD detectors were stored alternatingly in the first block of four histograms when the electric field was off and the second block of four histograms when the electric field was on. Measurements were performed for two electric fields: $E = 500/3$ V/mm and $E = 800/3$ V/mm (i.e., 500 or 800 V applied to a 3-mm-thick sample).

## III. ANALYSIS AND MODELS

ZF $\mu$SR allows the determination of internal magnetic fields at the position in the lattice where the muons stop. For a polycrystalline sample with a given static magnetic field $B$ at the stopping site of the muon, the muon depolarization function[14] may be expressed as $G_B(t) = \frac{1}{3} + \frac{2}{3}\cos(\gamma_\mu B t)$, where $\gamma_\mu = 2\pi \times 135.53$ MHz/T is the gyromagnetic ratio of the muon. $G_B(t)$ consists of two parts: a constant fraction of 1/3 and a fraction of 2/3 oscillating with the frequency $\omega = \gamma_\mu B$. For a given magnetic-field distribution $P(B)$, the muon depolarization function at the muon site is[17]

$$G_P(t) = \frac{1}{3} + \frac{2}{3}\int_0^\infty P(B)\cos(\gamma_\mu B t)dB. \qquad (1)$$

The function $P(B)$ contains information on the magnetic structure and the spatial magnetic-field distribution of the sample, but also on the effect of a static electric field $E$ on the local magnetic fields in the sample.

Due to an additional isotropic dynamic muon relaxation and the presence of a Cu background signal, the ZF depolarization function for $Cu_2OSeO_3$ is best described by the following equation:

$$A(t) = A_S\left(\frac{1}{3} + \frac{2}{3}\int_0^\infty P(B)\cos(\gamma_\mu B t + \phi)\,dB\right)e^{-\lambda t} + A_{Bg}\,G_{\mathrm{KT}}(\sigma_{Bg}t)\,e^{-\lambda_{Bg}t}. \qquad (2)$$

Here $A_S$ is proportional to the fraction of muons stopping in the sample, and $A_{Bg}$ is proportional to the fraction of muons stopping in the Cu sample holder. The parameters $\lambda_{Bg}$ and $\sigma_{Bg}$ describe the temperature-independent muon depolarization in Cu, while $\lambda$ corresponds to the dynamic muon relaxation in the sample. $G_{\mathrm{KT}}(\sigma_{Bg}t)$ denotes the Gaussian Kubo-Toyabe depolarization function.[18] Note that the phase $\phi = 0$ for a ZF. As for a powder sample, we observe also for the present single-crystal sample a static fraction of 1/3 for the depolarization function and an oscillating fraction of 2/3.[14] In the case of a single-crystal sample, though, these fractions are due to the formation of magnetic domains with a random spatial distribution, which in fact corresponds to the situation for a polycrystalline sample. Consequently, the angles between magnetic and electric polarizations are random. The best fit of $P(B)$ to the experimental data with a minimal set of parameters was obtained with a sum of two Gaussians:

$$P(B) = \sum_{i=1,2}\frac{F_S^i}{\sqrt{2\pi}\sigma_i/\gamma_\mu}\exp\left[-\frac{1}{2}\left(\frac{B-B_i}{\sigma_i/\gamma_\mu}\right)^2\right]. \qquad (3)$$

Here $F_S^1$ and $F_S^2$ are the fractions of the two Gaussians with mean fields $B_1$ and $B_2$ and standard deviations $\sigma_1/\gamma_\mu$ and $\sigma_2/\gamma_\mu$. Analysis of the data measured with the highest statistics ($100 \times 10^6$ positron events) at 10 K with Eqs. (2) and (3) (see Figs. 2 and 3) yields $F_S^1 = 0.18(2)$, $F_S^2 = 0.82(2)$, and $B_2/B_1 = 1.07(2)$ (note that $F_S^1 + F_S^2 = 1$). The fitting was performed by keeping all the sample parameters ($A_S$, $\sigma_1$, $\sigma_2$, $\lambda$, $F_S^1$, $F_S^2$, and $B_2/B_1$) and the background parameters ($A_{Bg}$, $\sigma_{Bg}$, and $\lambda_{Bg}$) the same, while $B_1(0\ \mathrm{V})$ and $B_1(500\ \mathrm{V})$ (data without and with the applied electric field) were free parameters. The temperature-independent sample asymmetry $A_S = 0.144$ and the background parameters $A_{Bg} = 0.05$, $\sigma_{Bg} = 0.14(2)\ \mu\mathrm{s}^{-1}$, and $\lambda_{Bg} = 0.11(2)\ \mu\mathrm{s}^{-1}$ were determined from the global fit of the whole temperature dependence, while the total initial asymmetry $A_S + A_{Bg} = 0.194$ was determined above $T_c$. Further more, all the background parameters, and the sample parameters $F_S^1$, $F_S^2$, and $B_2/B_1$, were kept as temperature independent.

Figure 2 shows the asymmetry time spectra at 10 and 58 K (below and above the magnetic transition) with and without electrostatic field $E$. The corresponding fits using Eqs. (2) and (3) are represented by the lines. Figure 3 shows the Fourier transform (FT) amplitudes of the oscillating part of the $\mu$SR spectra and the fitted curves shown in Fig. 2. For a low relaxation rate $\lambda$ these FT amplitudes represent the magnetic-field distribution $P(B)$ given by Eq. (3). Note that $P(B)$ consisting of two Gaussians [Eq. (3)] describes the

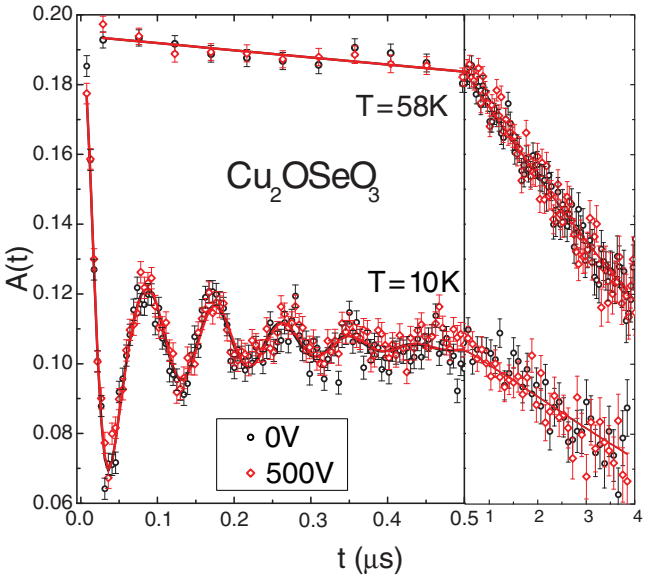


FIG. 2. (Color online) $\mu$SR time spectra of $Cu_2OSeO_3$ at 10 and 58 K in a ZF with ($\diamond$) and without ($\circ$) an applied electrical field $E = 500/3$ V/mm. Solid lines are fits to the data using Eqs. (2) and (3).

basic features of the $\mu$SR spectrum quite well, and that the FT amplitudes for $E = 0$ and $E = 500/3$ V/mm are almost identical.

Before presenting the experimental results, we describe below the relation between the measured $\mu$SR spectra and the magnetic structure of $Cu_2OSeO_3$. The crystal symmetry of $Cu_2OSeO_3$ is cubic, with a lattice constant $a = 8.9111$ Å and spatial group symmetry $P2_13$.[9] The lattice structure is thus quite complex, with 32 oxygen ions in the unit cell, suggesting quite a large number of possible muon stopping sites. Generally, the positive muon stops at a high symmetry interstitial site of the lattice, close to negatively charged ions (in this case $O^{2-}$). In some cases the muon may form

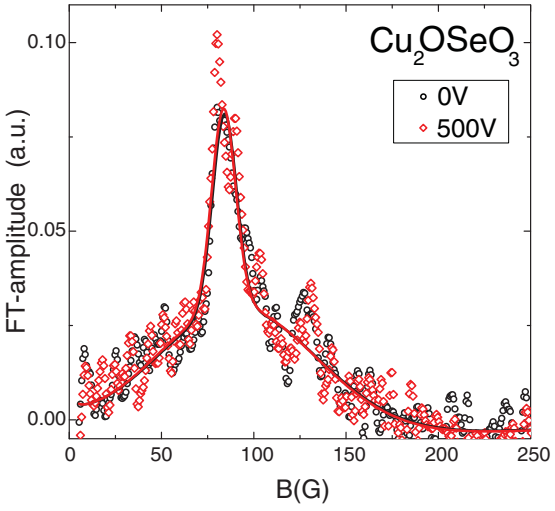


FIG. 3. (Color online) Fourier transform of the oscillating part of the asymmetry spectra shown in Fig. 2 [(black) circles, $E = 0$; (red) diamonds, $E = 500/3$ V/mm]. Solid lines are the FT of the corresponding solid curves in Fig. 2.

weak bonds with oxygen.[14] The function $P(B)$ describes the muon-site-weighted distribution of internal fields in the sample.

In order to find the muon stopping sites, an analysis of the electrostatic potential was performed. The potential at position $\mathbf{r}$ within the lattice unit cell was approximated using a spherical point charge-like model (in dimensionless units):

$$V(\mathbf{r}) = \sum_j \left( \frac{q_j}{R_j} + \frac{V_{xc}^0}{R_j} e^{-2R_j/R_j^I} \right). \quad (4)$$

The first term is the Coulomb potential, while the second term is the exchange correlation potential, which is usually assumed to be proportional to the local charge density [the expression $\exp(-R_j/R_j^I)$ represents an average radial wave function].[19,20] Here, $R_j = |\mathbf{r} - \mathbf{r}_j|$, and the sum is taken over ion coordinates $\mathbf{r}_j$ within a cluster of $4 \times 4 \times 4$ unit cells. The charges $q_j$ and the ionic radii $R_j^I$ are $+2$ and 0.71 Å, $+4$ and 0.42 Å, and $-2$ and 1.3 Å for Cu, Se, and O ions, respectively (here the elementary charge is unity). The adjustable parameter $V_{xc}^0$ was chosen as $\simeq +10$. Note that $V_{xc}^0 = 14$ corresponds to the condition where an attractive Coulomb potential of $O^{2-}$ equals the repulsive exchange correlation potential at distance corresponding to the oxygen ionic radius $R^I(O^{2-}) = 1.3$ Å. We found that the coordinates of the potential minima do not appreciably depend on $V_{xc}^0$ over a broad range of values. The potential $V(\mathbf{r})$ has five magnetically nonequivalent minima with nearly equal depths at the following sites: A = (0.215, 0.700, 0.970), B = (0.035, 0.720, 0.805), C = (0.195, 0.555, 0.795), D = (0.275, 0.295, 0.460), and E = (0.635, 0.550, 0.525). Sites A–E are indicated as red spots in Fig. 4. In addition, there are four local minima with a higher energy and lower probability of being occupied.

The muon probes the vector sum of the internal (dipolar) magnetic field and the contact field at a particular lattice cite. The dipolar magnetic field $\mathbf{B}(\mathbf{r})$ at position $\mathbf{r}$ within the lattice unit cell is calculated as follows:[21]

$$B_{\rm dip}^{\alpha}(\mathbf{r}) = \frac{\mu_0}{4\pi} \sum_{i,\beta} \frac{m_i^{\beta}}{R_i^3} \left( \frac{3R_i^{\alpha} R_i^{\beta}}{R_i^2} - \delta^{\alpha\beta} \right). \quad (5)$$

Here $\mathbf{R}_i = \mathbf{r} - \mathbf{r}_i$, $\alpha$ and $\beta$ denote the vector components $x$, $y$, and $z$, $\mathbf{r}_i$ is the position of the $i$th magnetic ion in the unit cell, and $m_i^{\beta}$ is the corresponding dipolar moment. The summation is taken over a sufficiently large Lorentz sphere of radius $R_L$. Beyond the Lorentz sphere, the integration is carried out over the domain volume. The contribution to the internal magnetic field from this integral is $\mathbf{B}' = 4\pi\mu_0(\frac{1}{3} - \hat{\mathbf{N}}_{\mathbf{d}})\mathbf{M}$,[22] where $\mu_0\mathbf{M} \simeq 66$ mT is the domain magnetization, and $\hat{\mathbf{N}}_{\mathbf{d}}$ the demagnetization tensor determined by the geometry of the domain and the magnetic anisotropy. For calculation of the magnetization, the lattice constant $a = 8.911\,13$ Å and the magnetic moment of $0.5\mu_B$ per $Cu^{2+}$ ion were taken from Ref. 9. For a magnetically isotropic spherical domain, $\hat{\mathbf{N}}_{\mathbf{d}} = \frac{1}{3}$.[21,22] Field $\mathbf{B}'$ and stray fields due to the neighboring domains average statistically to 0. They only give rise to an additional broadening of $P(B)$, which is smaller than the width of the narrow component of $P(B)$ (see Fig. 3). The magnetic structure of $Cu_2OSeO_3$ and the spatial magnetic-field

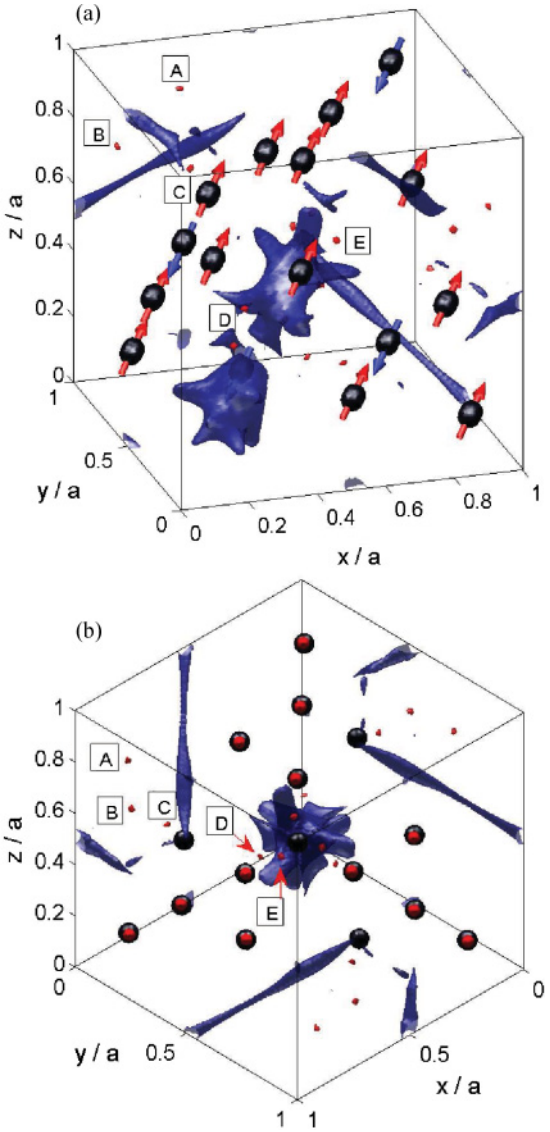


FIG. 4. (Color online) (a) Magnetic structure and dipolar fields in $Cu_2OSeO_3$.[9] Black spherical surfaces represent a field strength of 20 T (i.e., $Cu^{2+}$ ions). Arrows indicate magnetic moments of $Cu^{2+}$. Blue surfaces represent internal fields of 10 mT (for $0.5\mu_B$ per Cu ion). Red spots A–E are muon stopping sites. (b) The same as (a) but in the (111) direction.

distribution calculated with Eq. (5) are shown in Fig. 4. The probability field distributions for the magnetic structure with equal weights for muon sites A–E are shown in Fig. 5. Calculations were performed with Gaussian sampling around points A–E, with a standard deviation $\sigma_L = 0.23$ Å. Thus, the widths of the curves in Fig. 5 are proportional to the magnetic-field gradients at the corresponding sites. The total-field distribution from all sites A–D has a broad Gaussian-like shape centered at approximately 100 mT. This broad distribution agrees quite well with the experimental distribution (see Fig. 3). The narrow peak calculated for site E is located at about 15 mT, in contrast to the experimentally observed peak at around 85 mT. This discrepancy may be explained by assuming an additional contact field of approximately 70 mT at muon site E, resulting in a peak position of 85 mT (the total field is the vector sum

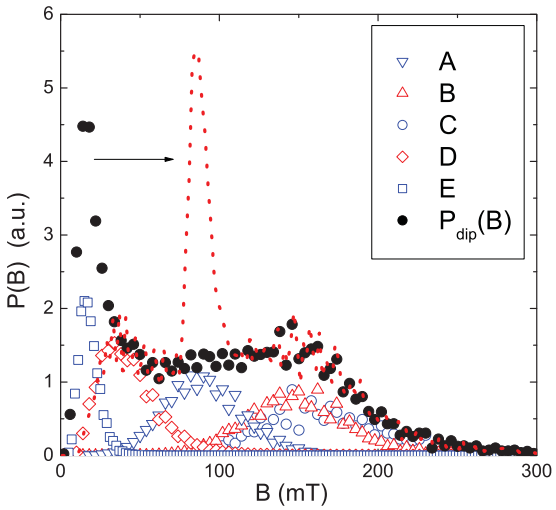


FIG. 5. (Color online) Probability distribution of dipolar fields $P_{\rm dip}(B)$ with equal weights for sites A–E (•). Contributions of the individual sites A, B, C, D, and E to $P_{\rm dip}(B)$ are represented by the symbols ▽, △, ○, ◇, and □, respectively. The width of each curve is proportional to the magnetic-field gradient at the corresponding site. The dotted line shows the $P_{\rm dip}(B)$ with an additional contact field of 70 mT at site E.

of dipolar field $\mathbf{B}_{\rm dip}$ and contact field $\mathbf{B}_c$). Note that the ratio of the broad to the narrow signal intensities is about 4, in good agreement with the ratio $F_S^2/F_S^1 = 4.5(5)$ obtained from Eq. (3).

## IV. RESULTS AND DISCUSSION

The temperature dependences of parameters $\sigma_1$, $\sigma_2$, and $\lambda$ as obtained from data analysis by means of Eqs. (2) and (3) are displayed in Fig. 6. The parameters $\sigma_1$ and $\sigma_2$ decrease with increasing temperature and drop to 0 at the Curie temperature $T_c = 57.0(1)$ K of the ferrimagnetic transition of $Cu_2OSeO_3$. The longitudinal relaxation rate $\lambda$ is a measure of the internal magnetic-field dynamics and can be expressed by the field-field correlation function $\lambda = \gamma_\mu^2 \int_0^\infty \langle B_\perp(t) B_\perp(0)\rangle dt$.[23] Here $B_\perp$ is the field component perpendicular to the muon-spin direction at the muon site. Brackets denote statistical averages. In the paramagnetic state close to $T_c$ the relaxation rate $\lambda$ is a measure of the spatial correlation length $\xi$ of the magnetic order. In the critical state the following relations hold: $\lambda \propto \xi^{3/2}$ for ferromagnets and $\lambda \propto \xi^{1/2}$ for antiferromagnets.[24–26] Note that these relations are strictly valid only in the critical regime very close to $T_c$. However, it was found empirically, that these relations describe experimental data rather well for EuO, EuS, and $RbMnF_3$ up to $\sim 1.3T_c$.[25,26] Above $T_c$ the correlation length $\xi$ follows the power law $\xi \propto (T/T_c - 1)^{-\tilde{\nu}}$, where the effective critical exponent $\tilde{\nu} \simeq 0.70$ for a three-dimensional (3D) Heisenberg magnet.[24–26] A fit of $\lambda$ above $T_c$ to the equation $\lambda(T) = A(T/T_c - 1)^{-\tilde{\omega}}$ results in $A = 0.0030(5)$ $\mu s^{-1}$ and the effective dynamic exponent[29] $\tilde{\omega} = 1.06(9)$ [see the solid (black) line in Fig. 6]. Thus, for $\tilde{\nu} \simeq 0.70$, we find with $\tilde{\omega}/\tilde{\nu} = 1.5$ that $\lambda \propto \xi^{1.5}$, in fair agreement with the critical behavior of a 3D ferromagnet ($\lambda \propto \xi^{3/2}$).

Next we discuss the $\mu$SR experiments with an electric field applied. The temperature dependence of the mean internal

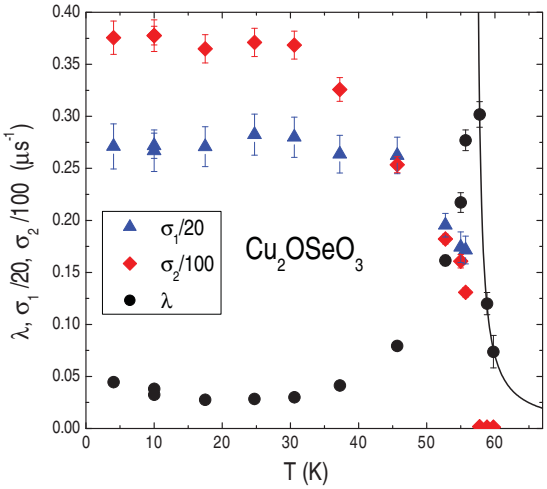


FIG. 6. (Color online) Transverse relaxation rates $\sigma_1$ and $\sigma_2$ as well as the longitudinal relaxation rate $\lambda$ of single-crystal $Cu_2OSeO_3$ as a function of temperature. The solid (black) line represents a fit of the data to the power law $\lambda(T) = A(T/T_c - 1)^{-\tilde{\omega}}$ (see text).

magnetic field $B_1$ with or without applied electric field $E$ is shown in Fig. 7(a). The temperature dependence of the internal magnetic field (i.e., the magnetic order parameter) decreases with increasing temperature and vanishes at $T_c$. Analyzing the data with the power law,[23]

$$B_1 = B_1(0)[1 - (T/T_c)^{\tilde{\alpha}}]^{\tilde{\beta}} \quad (6)$$

yields $T_c = 57.0(1)$ K, $\tilde{\alpha} = 2.00(9)$, $\tilde{\beta} = 0.39(1)$, and $B_1(0) = 85.37(25)$ and $85.57(25)$ mT for $E = 0$ and $500/3$ V/mm, respectively. The value of the effective critical exponent[29] $\tilde{\beta}$ lies quite close to the critical exponent $\beta \simeq 1/3$ expected for a 3D magnetic system.[27] For $T \to 0$ the temperature dependence of the internal field $B_1(0) - B_1(T) \propto T^{\tilde{\alpha}}$ is determined by the excitation of the ground-state magnetic order.[27,28] Figure 7(b) shows the difference $\Delta B_V = B_1(0\text{ V}) - B_1(500\text{ V})$ as a function of temperature. Obviously, the data points scatter substantially. However, a close examination shows that the data points below 50 K are systematically shifted to negative values, except for a point at 10 K [open (blue) circle in Fig. 7(b)], which is the first measured point and was recorded in the test phase of the experiment. Thus, we cannot exclude additional systematic errors related to instrument setup for the first point. The statistical average of all values of $\Delta B_V$ is 0 within error. By excluding the data point at 10 K the average value $\overline{\Delta B_V}$ below 50 K was found to be $\simeq -0.4(4)$ mT. These experiments suggest the presence of a small electric-field effect on the magnetic state of $Cu_2OSeO_3$.

Additional $\mu$SR experiments were performed with an applied transverse magnetic field (TF). The $\mu$SR spectra were found to be well described by the asymmetry function:

$$A_{\rm TF}(t) = \hat{A}_S \exp\left(-\frac{1}{2}\hat{\sigma}_2^2 t^2\right)\cos(\gamma_\mu \hat{B}_2 t + \phi) + \hat{A}_{Bg}\exp\left(-\frac{1}{2}\hat{\sigma}_{Bg}^2 t^2\right)\cos(\gamma_\mu \hat{B}_{Bg} t + \phi). \quad (7)$$

Parameter $\hat{A}_S(\hat{A}_{Bg})$ corresponds to $A_S(A_{Bg})$ in Eq. (2), while $\hat{\sigma}_2(\hat{\sigma}_{Bg})$ and $\hat{B}_2(\hat{B}_{Bg})$ are the relaxation rate and the mean field of the sample (Cu background), respectively. The values of $\hat{\sigma}_2$ and $\sigma_2$ were found to be approximately the same, and the Cu relaxation rate $\hat{\sigma}_{Bg} \simeq 0.25\ \mu s^{-1}$ is low. $\hat{B}_2$ is slightly larger than the applied field, while $\hat{B}_{Bg}$ is close to the applied field. In the TF $\mu$SR experiments the electric-field amplitude was increased to 800/3 V/mm. Note that the signal from the sample is well described by a single Gaussian and that the narrow signal in Eq. (3) broadens. The field dependence of $\Delta B'_V = \hat{B}_2(0\text{ V}) - \hat{B}_2(800\text{ V})$ at $T = 10$ K is shown in Fig. 7(c). No effect of the electric field $E$ on the internal magnetic field was found within the precision of the experiment, although a strong field dependence of the magnetocapacitance was reported.[9] The TF $\mu$SR experiment is less precise than the ZF experiment, since the narrow signal that mainly determines the errors becomes broader upon application of a magnetic field.

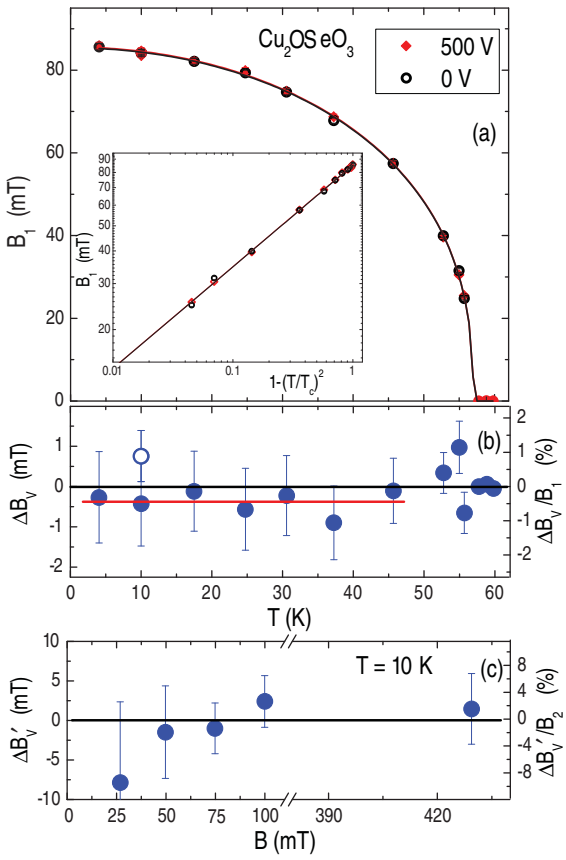


FIG. 7. (Color online) (a) Temperature dependence of the mean internal $B_1$ field in single-crystal $Cu_2OSeO_3$ for zero and applied electrostatic field $E$. Solid lines are power law fits to the data with Eq. (6). Inset: $B_1$ vs $[1 - (T/T_c)^2]$ on a log-log scale. (b) Electric-field shift $\Delta B_V = B_1(0\text{ V}) - B_1(500\text{ V})$ as a function of temperature. The lower solid horizontal (red) line corresponds to the mean value of $\overline{\Delta B_V} \simeq -0.4(4)$ mT below 50 K. (c) Electric-field shift $\Delta B'_V = \hat{B}_2(0\text{ V}) - \hat{B}_2(800\text{ V})$ as a function of the magnetic field measured in the TF $\mu$SR experiment at 10 K.

## V. CONCLUSION

In conclusion, we have performed a detailed investigation of magnetism and the magnetoelectric effect in $Cu_2OSeO_3$ by

ZF and TF $\mu$SR. An internal magnetic field $B_{\rm int}(T=0) = 85.37(25)$ mT was detected below $T_{\rm c} = 57.0(1)$ K, consistent with a ferrimagnetic state.[9] The effective critical exponent for the temperature dependence of $B_{\rm int}$ was found to be $\tilde{\beta} \simeq 0.39(1)$, in fair agreement with the critical exponent $\beta \simeq 1/3$ expected for 3D magnetic systems. The magnetic order parameter $B(0) - B(T) \propto T^2$ was found to exhibit a quadratic temperature dependence for $T \to 0$. The temperature dependence of the muon relaxation rate above $T_{\rm c}$ is well described by the relation $\lambda \propto (T/T_{\rm c} - 1)^{-\tilde{\omega}}$ with $\tilde{\omega} = 1.06(9)$, suggesting $\lambda \propto \xi^{3/2}$ ($\xi$ is the magnetic correlation length), which is characteristic for 3D ferromagnets.[24,25] ZF $\mu$SR measurements of the microscopic internal-field distribution with and without applied electric field $E = 500/3$ V/mm indicate a small electric-field effect on the internal magnetic field: $\Delta B_V = B_1(0\ \text{V}) - B_1(500\ \text{V}) = -0.4(4)$ mT. The strong muon relaxation sets a limit on the precision of detecting a magnetoelectric effect. To improve the precision of the $\mu$SR experiment substantially higher statistics would be needed.

## ACKNOWLEDGMENTS

We are grateful to A. Amato and A. Raselli for their technical support during the $\mu$SR experiments. Discussions with P. F. Meier on possible muon sites are acknowledged. This work was performed at the Swiss Muon Source (S$\mu$S), Paul Scherrer Institut (PSI), Switzerland). We acknowledge support by the Swiss National Science Foundation and the NCCR project "Materials with Novel Electronic Properties" (MaNEP).

*alexander.m@physik.uzh.ch

[1] M. Fiebig, J. Phys. D **38**, R123 (2005).
[2] N. A. Spaldin and M. Fiebig, Science **309**, 391 (2005).
[3] W. Eerenstein, N. D. Mathur, and J. F. Scott, Nature **442**, 759 (2006).
[4] S.-W. Cheong and M. Mostovoy, Nat. Mater. **6**, 13 (2007).
[5] N. A. Hill, J. Phys. Chem. B **104**, 6694 (2000).
[6] G. A. Gehring, Ferroelectrics **161**, 275 (1994).
[7] I. A. Sergienko and E. Dagotto, Phys. Rev. B **73**, 094434 (2006).
[8] H. Katsura, N. Nagaosa, and A. V. Balatsky, Phys. Rev. Lett. **95**, 057205 (2005).
[9] J.-W. G. Bos, C. V. Colin, and T. T. M. Palstra, Phys. Rev. B **78**, 094416 (2008).
[10] H. Effenberger and F. Pertlik, Monatsch. Chem. **117**, 887 (1986).
[11] V. P. Gnezdilov, K. V. Lamonova, Yu. G. Pashkevich, P. Lemmens, H. Berger, F. Bussy, and S. L. Gnatchenko, Fiz. Niz. Temp. **36**, 688 (2010) [Low Temp. Phys. **36**, 550 (2010)].
[12] K. H. Miller, X. S. Xu, H. Berger, E. S. Knowles, D. J. Arenas, M. W. Meisel, and D. B. Tanner, Phys. Rev. B **82**, 144107 (2010).
[13] V. Gnezdilov, K. Lamonova, Y. Pashkevich, P. Lemmens, H. Berger, F. Bussy, and S. Gnatchenko, Fiz. Nizk. Temp. **36**, 688 (2010).
[14] S. J. Blundell, Contemp. Phys. **40**, 175 (1999).
[15] D. G. Eshchenko, V. G. Storchak, and G. D. Morris, Phys. Lett. A **264**, 226 (1999).
[16] H. J. Lewtas, T. Lancaster, P. J. Baker, S. J. Blundell, D. Prabhakaran, and F. L. Pratt, Phys. Rev. B **81**, 014402 (2010).
[17] P. Carretta and A. Keren in *Highly Frustrated Magnetism*, ed. C. Lacroix, P. Mendels, and F. Mila (Springer-Verlag, Berlin, Heidelberg, 2011).
[18] R. Kubo, Hyperfine Interact. **104**, 3 (1997).
[19] S. Estreicher and P. F. Meier, Phys. Rev. B **27**, 642 (1983).
[20] G. J. M. Velders and D. Feil, Acta Crystallogr. Sec. B **45**, 359 (1989).
[21] S. J. Blundell, Physica B **404**, 581 (2009).
[22] R. M. White, *Quantum Theory of Magnetism* (McGraw-Hill, New York, 1970).
[23] F. L. Pratt, P. M. Zieliński, M. Balanda, R. Podgajny, T. Wasiutyński, and B. Sieklucka, J. Phys. Condens. Matter **19**, 456208 (2007).
[24] A. Yaouanc, P. Dalmas de Réotier, and E. Frey, Phys. Rev. B **47**, 796 (1993).
[25] S. W. Lovesey and E. Engdahl, J. Phys. Condens. Matter **7**, 769 (1995).
[26] S. W. Lovesey, B. Balcar, and A. Cuccoli, J. Phys. Condens. Matter **7**, 2615 (1995).
[27] L. J. De Jongh and A. R. Miedema, Adv. Phys. **23**, 1 (1974).
[28] L. P. Le, A. Keren, G. M. Luke, W. D. Wu, Y. J. Uemura, M. Tamura, M. Ishikawa, and M. Kinoshita, Chem. Phys. Lett. **206**, 405 (1993).
[29] H. Keller and I. M. Savić, Phys. Rev. B **28**, 2638 (1983).